Output-Feedback Control of Precision Motion Systems with Uncertain Nonlinearities

Mohammad Al Janaideh, Almuatazbellah M. Boker, and Micky Rakotondrabe

December 10, 2020

M. Al Janaideh is with the Department of Mechanical Engineering, Memorial University, St. John's, Newfoundland A1B 3X5, Canada, maljanaideh@mun.ca

A. M. Boker is with Bradley Department of Electrical and Computer Engineering, Virginia Tech, Blacksburg, VA 24060, USA, boker@vt.edu

M. Rakotondrabe is with Laboratoire Génie de Production, National School of Engineering in Tarbes (ENIT) / Toulouse INP, University of Toulouse, Tarbes France, mrakoton@enit.fr

Abstract

We propose output-feedback tracking control with an extended high-gain observer-based feedback control for a class of precision motion systems that include unknown rate-dependent hysteresis nonlinearities with linear dynamics. The proposed control system has a number of features; namely, (i) it can guarantee ultimate boundedness of the tracking error, where the ultimate bound can be made arbitrarily small, for any given initial conditions and for bounded unknown exogenous inputs and modeling parameters, (ii) it provides the possibility of shaping the transient response of the closed-loop system as desired, and (iii) the proposed technique is non-adaptive inversion free technique. To verify the effectiveness of these results, first simulation results are provided for an iron pendulum in a magnetic field system. Then, the output-feedback approach is also applied experimentally to a piezotube micropositioning actuator for a precision motion control.

1 Introduction

Considerable continuing efforts are being made to seek control methods for motion systems exhibiting strong hysteresis nonlinearities to perform high precision motion. Most of the actuators in these systems use smart or active materials: piezoelectric actuators, magnetostrictive actuators, and electroactive polymers [1]. Piezoelectric material-based actuators have been recently

used in different precise positioning systems since they can perform high resolution of movement at high excitation frequencies [2]. Moreover, these actuators have been used to design different nanopositioning systems, see for example [3]. Precise positioning driven by piezoelectric materials are found in various applications and some of them are now commercially available. For example, these applications include the Atomic Force Microscopy (AFM) [4], energy harvesting [5], piezoelectrically actuated hydraulic valves [6], diesel injectors [7], medical microrobots [8], nanomanipulator actuators [9], piezoelectric flexible manipulator [10], manipulator grippers[11].

In [4], a piezoceramic actuator is used to design a micro-air vehicle. A homogenized energy model is developed to characterize the dynamic of the used actuators. In [5], a multistage energy harvester is designed with a piezoelectric stack to enhance the power output from human footstep during walking. In [6] a piezoelectric ring bender is proposed to control a high pressure hydraulic actuation system to improve the accuracy and performance of the flow. In [7], a piezoceramic actuator is used to design a diesel injector system with a high level of accuracy. The study showed that piezoceramic actuator systems can be integrated with hydraulic injectors. In [8], piezoceramic materials are used to design a kinematic microrobot devoted to laser phonosurgery tasks. The study showed the advantage of using the piezoceramic materials in microrobots. In [9], a multi-degree of freedom nano-manipulator is designed with piezoceramic actuators to obtain high precision system with large range and high mechanical bandwidth. In [10], simultaneous positioning control and vibration suppression of flexible manipulator is accomplished with a piezoelectric actuator. In [11], piezoelectric materials are used to design heavy force-moment sensor to detect forces of heavy-load manipulator's gripper.

Hysteresis nonlinearities that characterize the nonlinear dynamics of these actuators, principally piezoelectric and magnetostrictive ones, considerably degrade the tracking performance, cause high oscillations, and reduce the accuracy of these micro/nano-positioning tasks [12]. Thus, considerable works have been led in the modeling and control of piezoelectric actuators by accounting for their hysteresis nonlinearities in order to reach certain accuracy in the final tasks. Within the last years, extension of these works have been raising in order to consider the fact that the hysteresis nonlinearities are also strongly dependent on the rate of the input control, i.e. the nonlinearities are dynamical. Overall, these extension can be classified into two categories. The first category consists in simplifying the nonlinear dynamics into a rate-independent hysteresis (nonlinear statics) followed by a linear dynamics, which is inspired from the well-known Hammerstein architecture. In this category, the classical Bouc-Wen [13], the Prandtl-Ishlinskii model [14] and the Preisach model [15] were the most used as the rate-independent hysteresis. Different adaptive and robust control techniques have been proposed in the literature to control

and stabilize dynamical systems coupled with rate-independent hysteresis nonlinearties. These include Preisach hysteresis with a linear dynamical system [16], Prandtl-Ishlinskii hysteresis with a nonlinear dynamical system [17], and Prandtl-Ishlinskii hysteresis with with a linear dynamical system [18].

The second category considers the rate-dependent hysteresis nonlinearties, where the hysteresis models parameters include the time rate of the applied input. The Prandtl-Ishlinskii approach has undergone extensive studies for its extension to rate-dependent models last few years, for example the inverse rate-dependent Prandtl-Ishlinskii model with a piezoceramic actuator [19] and the inverse generalized Prandtl-Ishlinskii model with a magnetostrictive actuator [20]. In these studies, the rate-dependent Prandtl-Ishlinskii models and modified play-operators or stop-operators have been introduced. This paper is dealing with modeling a class of systems with rate-dependent hysteresis nonlinearities by proposing Netushil's principle and operator. The proposed rate-dependent hysteresis model is afterwards feedback controlled through a high-gain observer. Different control techniques have been proposed to stabilize dynamical systems with hysteresis. These techniques can be classified into inversion-based and inversion free-based control systems. Inversion-based control systems consider the inverse hysteresis model as a feedforward compensator to reduce the effect of hysteresis nonlinearities. These include inverse Preisach model, inverse Prandtl-Ishlinskii model, inverse rate-dependent Prandtl-Ishlinskii model, inverse generalized Prandtl-Ishlinskii model. These inverse models have been used with different control systems to enhance the performance of the compensation and to stabilize associated dynamical systems. These include robust control with inverse Prandtl-Ishlinskii model [21], PID control with inverse Prandtl-Ishlinskii model [22], disturbance observer with the inverse Prandtl-Ishlinskii model [23], and extended high-gain observer [24]. These techniques assume known hysteresis nonlinearties within the closed-loop control systems [24].

Other approaches fall under the inversion free-based control systems. These include disturbance rejection [25], hybrid control for backlash hysteresis operator [26], adaptive control for Prandtl-Ishlinskii model [27], passivity-based control for Preisach model [28], an inversion-free feedforward rate-dependent compensator for the rate-dependent Prandtl-Ishlinskii model [29], a multiplicative structure to compensate for the Bouc-Wen hysteresis nonlinearity in piezoelectric actuators [13], and adaptive control [30].

The main contributions of the paper include:

- Development of inversion-free adaptive-free control approach for a piezoceramic micro-positioning system that deals with uncertain hysteresis dynamics and high oscillations.
- Development of an extended high-gain observer-based control strategy to stabilize a wide

class of precision motion systems with detailed stability analysis and error boundedness with unknown hysteresis nonlinearties.

- Perform experimental study with a piezoceramic micro-positioning cantilever that shows rate-dependent hysteresis and high oscillations.

In summary, the main contribution of this paper is to show that an extended high-gain observer-based output-feedback control system can solve the tracking problem for a class of precision motion systems with unknown hysteresis nonlinearties in a way that does not need inverse hysteresis model nor adaptive techniques.

More specifically, the control strategy is based on employing a feedback linearization control assuming first that all the states as well as the hysteresis nonlinearity and exogenous inputs are known. This way, the transient performance can be shaped as desired by choosing the eigenvalues of the closed-loop system. Considering now the realistic scenario where only the measured output is available for feedback and that modeling of the system nonlinearities and exogenous inputs may not be precise, we utilize an extended high-gain observer to estimate the unavailable states and system nonlinearities. Using this approach, we show that the standard features of high-gain observer-based control systems are attainable. In particular, we show that the closed-loop system tracks any bounded reference signal in a robust way and for any given initial conditions. It is worth to note that in the literature, output feedback structure has already been used to control piezoelectric actuators. In [31], an output feedback controller was designed with a linear quadratic technique and was combined with a feedforward controller to damp the inherent badly damped vibration of the piezoelectric actuator. However, the hysteresis nonlinearity was not considered and therefore limited the application to piezoelectric actuator that work in low deformation/displacement only. In [32] and [33], output feedback controller designs based on linear quadratic (LQ) tracker technique and on poles assignment technique respectively have been proposed. Both of the two works utilized interval models to approximate the behavior of the piezoelectric actuator. Whilst the models accounted for parametric uncertainties, they still remained linear and the hysteresis nonlinearity was still not considered. Therefore, against the literature on output feedback control of piezoelectric actuators, the contribution of this paper is the design of controller with consideration of the hysteresis nonlinearity.

We also show that it is possible to design the controller in such a way that allows the closed-loop system to have desired transient performance. This latter feature distinguishes the proposed approach in this paper from a similar approach proposed in [34] applied to systems with rate-independent hysteresis. Moreover, it was shown in [34] that for the control system to handle unknown modeling parameters, it utilizes an auxiliary (dynamic) controller to compensate for the

unknown parameters. In this paper, on the other hand, we show that there is no need for that as the output feedback controller can be modified in a straight forward way to compensate for any unknown parameters. Preliminary results of this study were presented in [35].

The remainder of the paper is organized as follows. Section 2 introduces the problem formulation of the study, the Netushil hysteresis model, and the bounds of the model. In Section 3, a closed-loop system with the unknown hysteresis nonlinearities is considered. The section proposed the high-gain observer-based output feedback control for uncertain hysteresis and unknown uncertainties and disturbances. Section 4 considers tracking control of an iron pendulum in a magnetic field with the rate-dependent Netushil hysteresis model under different scenarios. Then section 5 presents experimental results of the proposed high-gain observer-based output feedback control with piezoelectric actuator classically employed in precise positioning applications such as in atomic force microscopy and in nanomanipulation. The piezoelectric actuator shows rate-dependent hysteresis, creep effects, and high oscillations. Finally, the conclusion and future work are presented in Section 6.

2 System Model and Problem Formulation

This section states the problem formulation.

2.1 Problem formulation

We consider precision motion systems represented by the following nonlinear model[1]

$$\begin{aligned}
\dot{x}_1 =& x_2, \\
\dot{x}_2 =& x_3, \\
&\vdots \\
\dot{x}_m =& a(x,w) + \psi(\eta) + \rho(t) + u,
\end{aligned} \tag{1}$$

$$\epsilon\dot{\eta} = \Phi(x,\eta), \tag{2}$$

$$\dot{w} = f_0(x,w), \tag{3}$$

$$y = x_1, \tag{4}$$

[1] Without loss of generality, the hysteresis model (2.1) can depend on the input u. This is in view of the fact that the control input is going to be designed as a globally bounded function of the state.

where $x \in \mathbb{R}^m$, $w \in \mathbb{R}^q$, $u \in \mathbb{R}$ and $y \in \mathbb{R}$ are the control input and measured output, respectively, $\psi(\eta)$ is a function that represents the output of the hysteresis dynamics and $\eta \in \mathbb{R}^n$ is the state of the hysteresis dynamics (Netushil hysteresis system), which will be described in more details in Subsection 2.2, ϵ is a positive small constant, $\rho(t) \in \mathbb{R}$ is an unknown bounded disturbance, and $a(\cdot,\cdot)$ and $f_0(\cdot,\cdot)$ are assumed to be sufficiently smooth and locally Lipschitz nonlinear functions (could be unknown). The equations $\epsilon\dot{\eta} = \Phi(0,\eta)$, and $\dot{w} = f_0(0,w)$ constitute the zero dynamics of the system, i.e. the remaining dynamics of the system when $y = 0$ [36]. Accordingly, the internal dynamics are based on the zero dynamics. It is worth noting that the system (1)-(4) is in the nonlinear normal form, where the output and its derivatives are the external dynamics and the η and w are the internal dynamics [36].

In Subsection 2.2, we will show that (2) is bounded-input-bounded state stable. We further assume that (3) is bounded-input-bounded state stable making the whole internal dynamics bounded-input-bounded state stable. More specifically, we have the following assumption. There is a continuously differentiable function $V_0(w)$, class K functions β_1 and β_2, and a nonnegative continuous non-decreasing function χ such that

$$\beta_1(||w||) \leq V_0(w) \leq \beta_2(||w||)$$
$$\frac{\partial V_0}{\partial w} f_0(x,w) \leq 0, \quad \forall\ ||w|| \leq \chi(||x||)$$

for all $x, w \in \mathbb{R}^m \times \mathbb{R}^q$.

We consider the problem of controlling the output $y(t)$ so that it asymptotically tracks a reference signal $d_1(t)$. In this case, we assume that $d_1(t)$ is a smooth bounded function and $d_2 \triangleq \frac{dd_1}{dt}$, $d_3 \triangleq \frac{dd_2}{dt}$, $\ldots$, $d_m \triangleq \frac{dd_{m-1}}{dt}$ to be bounded for all $t \geq 0$. The closed-loop system's transient response is desired to have some predefined characteristics such as particular settling time and percentage overshoot. Towards accomplishing this objective, we consider the change of variables

$$e = x - d,$$

where $e = [e_1\ e_2\ \ldots\ e_m]^T$, and $d = [d_1\ d_2\ \ldots\ d_m]^T$. Using this change of variables, we get the

tracking error dynamics

$$\dot{e}_1 = e_2, \tag{5}$$

$$\dot{e}_2 = e_3, \tag{6}$$

$$\vdots$$

$$\dot{e}_m = a(e + d, w) + \psi(\eta) + \rho(t) + u - \dot{d}_m, \tag{7}$$

$$\epsilon\dot{\eta} = \Phi(e + d, \eta), \tag{8}$$

$$\dot{w} = f_0(e + d, w), \tag{9}$$

$$y_t = e_1 = x_1 - d_1, \tag{10}$$

where y_t is the measured tracking error. The problem can now be cast as designing a controller u to asymptotically regulate $e(t)$ to zero while meeting certain requirements on the transient response.

2.2 The Hysteresis Model and its Properties

In this section, we present a rate-dependent hysteresis model using a singularly perturbed ordinary differential equation with a deadzone operator. Specifically, we consider Netushil's principle [37] to characterize a class of rate-dependent hysteresis nonlinearity in smart materials-based actuators.

2.2.1 Input-output relationship

It is important to mention that the Netushil's principle uses the slow-fast systems to represent hysteresis operators [38]. This model can characterize a class of rate-independent and rate-dependent hysteresis nonlinearities in smart materials-based actuators. However, the inverse model, which can be used as a feedforward compensator, is not available in the literature. Compared with other hysteresis models such as the Preisach model, Prandtl-Ishlinskii model, and Bouc-Wen model, the Netushil model includes a perturbation constant that can add uncertainties to the hysteresis curves [35]. A linear combination of weighted Netushil hysteresis operators can be presented as

$$\psi(\eta) = \sum_{i=0}^{n} p_i \eta_i, \tag{11}$$

where

$$\begin{aligned} \epsilon\dot{\eta}_i(t) &= \Phi_{r_i}[z_i](t), && (12)\\ z_i(t) &= v(t) - \eta_i(t) && (13)\\ \eta_i(0) &= \eta_{i0}, && (14) \end{aligned}$$

where $v \in \mathbb{R}$ is the input, $p_i \geq 0$ are positive constants, $i = 1, 2, \ldots, n$, $\eta_i(0)$ are initial conditions, $r_i \geq 0$, where $r_0 > r_1 > \cdots > r_n$ are thresholds that determine the radius of the hysteresis loops, and $\Phi_{r_i}[z_i](t)$ are the output of the deadzone operators, where

$$\Phi_{r_i}[z_i](t) = \begin{cases} z_i(t) - r_i & \text{for } \; z_i(t) > r_i \;\; \& \;\; \dot{v}(t) > 0, \\ 0 & \text{for } \; |z_i(t)| < r_i, \\ z_i(t) + r_i & \text{for } \; z_i(t) < -r_i \;\; \& \;\; \dot{v}(t) < 0. \end{cases} \tag{15}$$

As a result,

$$\epsilon\dot{\eta}_i(t) = \begin{cases} v(t) - \eta(t) - r_i & \text{for } \; z_i(t) > r_i \;\; \& \;\; \dot{v}(t) > 0, \\ 0 & \text{for } \; |z_i(t)| < r_i, \\ v(t) - \eta(t) + r_i & \text{for } \; z_i(t) < -r_i \;\; \& \;\; \dot{v}(t) < 0. \end{cases} \tag{16}$$

Then, for $z_i(t) > r_i$ and $\dot{v}(t) > 0$,

$$\epsilon|\dot{\eta}_i(t)| = v(t) - \eta_i(t) - r_i, \tag{17}$$

for $z_i(t) < -r$ and $\dot{v}(t) < 0$,

$$-\epsilon|\dot{\eta}_i(t)| = v(t) - \eta_i(t) + r_i, \tag{18}$$

and for $|z_i(t)| < r_i$,

$$-\epsilon|\dot{\eta}_i(t)| = 0. \tag{19}$$

Then, (i) for $\dot{v}(t) > 0$ and $z_i(t) > r_i$, we have $\eta_i(t) = v(t) - r_i - \epsilon|\dot{\eta}_i(t)|$ and $\eta_i(t) = v(t) - r_i(t)$, (ii) for $\dot{v}(t) < 0$ and $z_i(t) < -r_i$, we have $\eta_i(t) = v(t) + r_i(t)$, and (iii) for $|z_i(t)| < r_i$ and $\dot{v}(t) = 0$,

we have $\eta_i(t) = v(t) + r_i(t)$, where

$$r_i(t) = r_i + \epsilon|\dot{\eta}_i(t)|. \tag{20}$$

Here, we define $r_i(t)$ as the time-dependent threshold of the Netushil hysteresis operator. The above equation can characterize hysteresis under different operating conditions. At low excitation frequencies the threshold equation $r_i(t) \approx r_i$ and this represents the time independent hysteresis. At higher frequencies, the term $\epsilon|\dot{\eta}_i(t)|$ represents the rate-dependent hysteresis nonlinearties. This equation has been used to model the hysteresis and creep behavior in piezoelectric and magnetostrictive materials. Physically, we add a viscous element, $\epsilon|\dot{\eta}_i(t)|$, in the threshold equation to express the rate-dependent hysteresis. Equation (20) is equivalent to characterize rate-dependent by means of an analogical model with elastic, plastic, and viscous elements. More details can be found in [39, 40].

In this part we show how to find the actual input $v(t)$ of the proposed hysteresis model. The range of v should be not be smaller than the width ϱ of the observed hysteresis loop. For the Netushil hysteresis loop, we define its width as the largest separation between two input values that correspond to a same output value. The maximum width of the hysteresis loop is the separation between the increasing and decreasing curves when the hysteresis operators are on their increasing and decreasing curves curves, respectively. For the increasing curve, the output of Netushil hysteresis model can be expressed as $\psi(\eta(t)) = \sum_{i=1}^{n} p_i(v(t) - r_i(t))$; for the decreasing curve, the output can be expressed as $\psi(\eta(t)) = \sum_{i=1}^{n} p_i(v(t) + r_i(t))$. To figure out the horizontal separation of the input-output loop between these two curves we can find the input values, v^{*+} and v^{*-}, for both curves, with their corresponding outputs $\psi(\eta(t)) = 0$. By considering $r_1(t) \leq r_i(t) \leq r_n(t)$, for $i = 1, \cdots, n$, we can verify the Netushil hysteresis loop width as

$$\varrho = v^{*+} - v^{*-} = 2\frac{\sum_{i=1}^{n} p_i r_n^*}{\sum_{i=1}^{n} p_i},$$

where r_n^* is the threshold value of the maximum rate-dependant threshold $r_n(t)$ at $\psi(\eta(t)) = 0$ of increasing or decreasing curves. Then the range of the input v should be larger than ϱ.

2.2.2 Lipschitz continuity and bounds

In this section we show that the Netushil operator is a Lipshitz-continuous operator. For any i, let $\underline{f}_i = -\epsilon|\dot{\eta}_i(t)|$, $\bar{f}_i = \epsilon|\dot{\eta}_i(t)|$, and $f_i = 0$. Following [38], there exist two Lipshitz continuous increasing functions $\underline{f}_i(v(t)) > \bar{f}_i(v(t))$ such that $f > 0$ when $y > \bar{f}(v)$, $f = 0$, when $y \in$

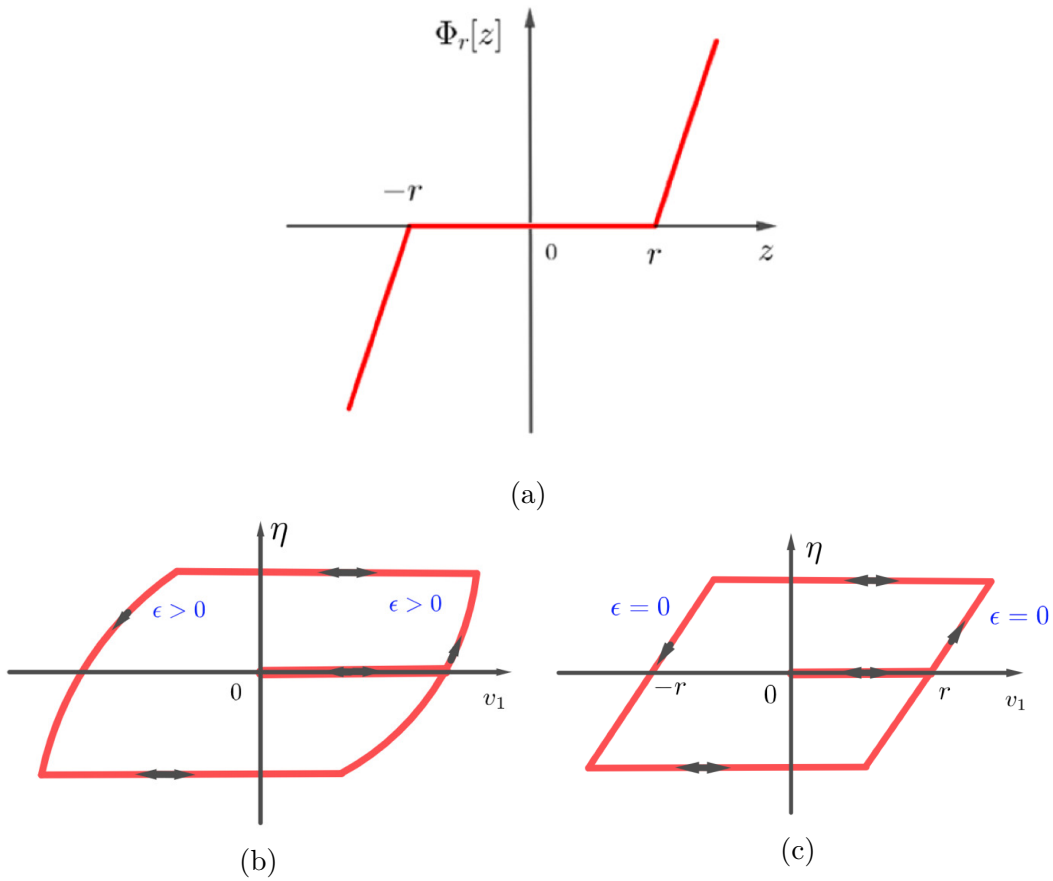

Figure 1: (a) Input-output relationship of a deadzone operator Φ_r of threshold r, input z, and output $\Phi_r[z]$. Input-output relationship of Netushil hysteresis operator with (b) $\epsilon > 0$, and (c) $\epsilon = 0$.

$[\bar{f}(v), \underline{f}(v)]$, and $f < 0$ when $y < \underline{f}(v)$. We can write

$$|f(t)| \leq np_{\max} \max\{|\eta_i(t)|\}, \tag{21}$$

where $p_{\max} = \max\{p_i\}$ and we have $\max\{|\eta_i(t)|\}$ with $r_i = 0$. Then $\epsilon\dot{\eta}(t) = v(t) - \eta(t)$, $\epsilon\dot{\eta}(t) = v(t) + \eta(t)$, and $\epsilon\dot{\eta}(t) = 0$. Since $0 < \epsilon << 1$, we can write $\eta_i(t) = v(t) + \sigma(t)$, where $\sigma(t)$ is the shift in the output $\eta(t)$ due to the term $\epsilon\dot{\eta}(t)$. Then, we can write

$$|\psi| \leq np_{\max}|v| + np_{\max}|\sigma|, \tag{22}$$

Then, the bounds of the model depends on the input $v(t)$ and ϵ.

Alternatively, we can show that the hysteresis model is bounded-input-bounded-state stable

when viewing $v(t)$ as input, which is a function of $e+d$ in view of (8). For this purpose, we consider the Lyapunov function $V_{1i}(\eta_i)=\frac{1}{2}\eta_i^2$. In view of (16), we can see that the derivative of $V_{1i}(\eta_i)$ takes the piecewise linear form

$$\begin{aligned}\dot{V}_{1i}=\eta_i\dot{\eta}_i &\leq \begin{cases} -\frac{1}{\epsilon}\eta_i^2+|\eta_i|(|v|-|r_i|), & \text{if} \quad \eta_i<v-r_i \;\&\; \dot{v}>0, \\ & \text{or if} \quad \eta_i>v+r_i \;\&\; \dot{v}<0, \\ 0, & \text{if} \quad |v-\eta_i|<r_i. \end{cases} \\ &\leq \begin{cases} -\frac{1}{2\epsilon}\eta_i^2, \quad \forall\, |\eta_i|\geq 2\epsilon(|v|-|r_i|), \text{ if} \quad \eta_i<v-r_i \;\&\; \dot{v}>0, \\ & \text{or if} \quad \eta_i>v+r_i \;\&\; \dot{v}<0, \\ 0, & \text{if} \quad |v-\eta_i|<r_i. \end{cases}\end{aligned} \tag{23}$$

The segment inequalities (23) imply that the internal dynamics (8) are bounded-input-bounded-state stable.

3 Extended High-gain Observer-Based Control

As a step towards solving the control problem, in what follows, we will design an extended high-gain observer to estimate the state vector e as well as the nonlinear and/or the unknown terms included in Equation (7). We will then design a stabilizing controller that makes use of the estimated information. As will be shown later, the estimation of the unknown functions is possible since we will assume that these collectively constitute an extended state of the system. This helps in mitigating any errors associated with the modeling process of the hysteresis and the modeling of the exogenous input. The choice of utilizing the extended high-gain observer is motivated by the fact that they can provide state estimates robustly and in relatively fast time. Furthermore, high-gain observers are known to have the ability to recover the performance of any stabilizing state-feedback controller [41], [42], [43], [44]. This property is beneficial in shaping the transient performance of the closed-loop system.

3.1 State-feedback Controller

Our choice of utilizing a high-gain observer implies that the estimates of e and $\kappa \triangleq a(e+d,w)+\psi(\eta)+\rho(t)-\dot{d_m}$ will be provided in a relatively fast time. As a result, we can design a controller as if this information is available for feedback. This leads to the feedback linearization control

$$u=-\kappa-k_1e_1-k_2e_2-\cdots-k_me_m. \tag{24}$$

The closed-loop system is then given by

$$\dot{e} = A_c e, \tag{25}$$

$$\epsilon\dot{\eta}_i = \Phi_{r_i}[e + d - \eta_i](t), \quad i = 1, 2, \ldots, n, \tag{26}$$

$$\dot{w} = f_0(e + d, w), \tag{27}$$

where

$$A_c = \begin{bmatrix} 0 & 1 & \ldots & \ldots & 0 \\ 0 & 0 & 1 & \ldots & 0 \\ \vdots & \vdots & \vdots & \ddots & \vdots \\ 0 & 0 & \ldots & \ldots & 1 \\ -k_1 & -k_2 & -k_3 & \ldots & -k_m \end{bmatrix} \in \mathbb{R}^{m\times m}$$

and $k_1, k_2, \ldots, k_m$ are positive constants chosen so that A_c has desired eigenvalues. Because the states and the disturbance are not available for feedback, we will utilize extended high-gain observer to provide estimates of the missing information in (24). This is possible because of two main features of the high-gain observer; namely, it is robust to modeling errors and relatively fast. We will show next that these two features can be achieved by selecting the gain sufficiently high. Thanks to this, the output feedback controller can recover the performance of the state feedback controller.

3.2 Extended High-gain Observer-based Output Feedback Control

Consider the system (5)-(7), then an extended high-gain observer can be given as

$$\dot{\hat{e}}_1 = \hat{e}_2 + \frac{\alpha_1}{\mu}(y_t - \hat{e}_1), \tag{28}$$

$$\dot{\hat{e}}_2 = \hat{e}_3 + \frac{\alpha_2}{\mu^2}(y_t - \hat{e}_1), \tag{29}$$

$$\vdots$$

$$\dot{\hat{e}}_m = \hat{\kappa} + u + \frac{\alpha_m}{\mu^m}(y_t - \hat{e}_1), \tag{30}$$

$$\dot{\hat{\kappa}} = \frac{\alpha_{m+1}}{\mu^{m+1}}(y_t - \hat{e}_1), \tag{31}$$

where $\mu > 0$ is a small parameter to be designed, y_t is given by (10) and $\alpha_1, \alpha_2, \ldots, \alpha_{m+1}$ are chosen such that the polynomial $s^{m+1} + \alpha_1 s^m + \alpha_2 s^{m-1} + \cdots + \alpha_{m+1} = 0$ is Hurwitz.

Let $\Omega \in \mathbb{R}^{(m+n+q)}$ be an arbitrarily large compact set that includes any given initial conditions of the closed-loop system (25)-(27). Combining the observer (28)-(31) with the control (24) leads

to the output-feedback control

$$u = M\text{sat}\left(\frac{-\hat{\kappa} - k_1 e_1 - k_2 \hat{e}_2 - \cdots - k_m \hat{e}_m}{M}\right), \tag{32}$$

where $\text{sat}(\cdot)$ is the saturation function. The saturation is used to protect the system from peaking in the observer's transient response [45]. The saturation limits $\pm M$ are chosen to be outside of the compact set Ω, according to

$$M > \max_{(e,\eta_i,i=1,2,\ldots,n)\in\Omega} | - \kappa - k_1 e_1 - k_2 \hat{e}_2 - \cdots - k_m \hat{e}_m|.$$

We will show later how one can practically choose the saturation limits. Notice that the output-feedback controller (32) does not require the knowledge of the derivatives of d_1. Then we now have the following result, which is a special case of the result reported in [46].

Theorem 3.1 *Consider the closed-loop system formed of the system* (5)-(10)*, the observer* (28)-(31) *and the controller* (32)*. Let Assumption 2.1 hold. Furthermore, let S be a compact subset of $\mathbb{R}^{m+1}$ and Ω_0 be a compact set in the interior of Ω. Then, for all initial conditions $(e(0), \eta_1(0), \eta_2(0)), \ldots, \eta_n(0), w(0)) \in \Omega_0$ and $(\hat{e}(0), \hat{\kappa}(0)) \in S$,*

- *there exits $\mu_1^* > 0$ such that for every $0 < \mu \leq \mu_1^*$, the trajectories of the closed-loop system are bounded for all $t \geq 0$;*
- *given any $\lambda_1 > 0$, there exits $\mu_2^* > 0$, dependent on λ_1, such that for every $0 < \mu \leq \mu_2^*$,*

  $$||e(t) - e_r(t)|| \leq \lambda_1, \quad \forall\, t \geq 0,$$

  where e_r is the solution of the target system (25) *with $e_r(0) = e(0)$.*
- *given any $\lambda_2 > 0$, there exits $\mu_3^* > 0$ and $T_1 > 0$, both dependent on λ_2, such that for every $0 < \mu \leq \mu_3^*$,*

  $$||e(t)|| \leq \lambda_2, \quad \forall\, t \geq T_1.$$

Proof: The proof of Theorem 3.1 follows closely the proof of Theorem 1 in [46]. Specifically, in this paper, there are two special cases to consider relative to [46]. First, part of the internal dynamics is the hysteresis model, which is based on a locally Lipschitz function and in view of (23) is shown to be bounded-input-bounded-state stable. Second, the control input coefficient is assumed to be known and constant. In fact, in this case, and without loss of generality, it is assumed to be equal to 1.

Consider now the closed-loop system (25)-(27). Given that A_c is Hurwitz by design, using the Lyapunonv function $V_2(e) = e^T P_1 e$ where $P_1 = P_1^T$ is the solution of the Lyapunov equation $P_1 A_c + A_c P_1 = -Q_1$, for some $Q_1 = Q_1^T > 0$, it is straight forward to show that the origin of (25) is exponentially stable. Moreover, Assumption (2.1) and (23) guarantee that the internal dynamics are bounded input-bounded-state stable when viewing $e + d$ as input. Consider next the change of variables

$$\xi_i = \frac{e_i - \hat{e}_i}{\mu^{m+1-i}}, \quad \text{for } 1 \leq i \leq m, \tag{33}$$

$$\begin{aligned} \xi_{m+1} &= a(e+d, w) + \psi(\eta) + \rho(t) - \dot{d}_m - \hat{\kappa} \\ &\triangleq \Delta(e, d, w, \eta, t) - \hat{\kappa}. \end{aligned} \tag{34}$$

Let $\xi = [\xi_1, \cdots, \xi_{m+1}]$. Using the change of variables (33)-(34), it can be shown that we have the fast dynamics

$$\mu \dot{\xi} = \Lambda \xi + \mu B \dot{\Delta}, \tag{35}$$

where

$$\Lambda = \begin{bmatrix} -\alpha_1 & 1 & \dots & \dots & 0 \\ -\alpha_2 & 0 & 1 & \dots & 0 \\ \vdots & \vdots & \vdots & \ddots & \vdots \\ -\alpha_m & 0 & \dots & \dots & 1 \\ -\alpha_{m+1} & 0 & 0 & \dots & 0 \end{bmatrix}, \quad B = \begin{bmatrix} 0 \\ 0 \\ \vdots \\ 1 \end{bmatrix} \in \mathbb{R}^{(m+1)},$$

and $\dot{\Delta}$, which is the derivative of the function Δ in (34), is a locally Lipschitz function bounded by $||\xi||$, uniformly of μ. Notice that Λ is a Hurwitz matrix by design.

It can be seen now that the closed-loop system (25)-(27) with the system (35) is in the standard form following the literature related to the high-gain observer [46]. Accordingly, for sufficiently small μ, it can be shown that ξ would be $\mathcal{O}(\mu)$, i.e. order of μ, after a short transient period of time. After this transient period, using Assumption 2.1 and (23) and the exponential stability of the origin of (25), the closed-loop system trajectories and ξ can be shown to belong to a positively invariant set establishing the boundedness of all the states. The second and third bullets can be established by following regular perturbation analysis, continuous dependence of the solutions of differential equations on initial conditions and parameters [[36], Theorem 9.1], and exponential stability of the origin of (25). □

Remark 3.1 *It is important to note that saturation is a standard tool used in conjunction*

with high-gain observers to guard the system from the negative effects of peaking [45]. In our case, it will not affect stability due to two reasons:

1. *The saturation is chosen so that it is only activated outside the domain of the states under state-feedback control. We show in Section 4 how this can be done.*

2. *The saturation will only be activated for a relatively short period of time as the peaking only happens due to the difference in initial conditions between the actual and estimated states. During this period, all the system states will be bounded. This period of time will get shorter as the observer parameter μ is chosen smaller. After this period, all the closed-loop system states enter into a stable positively invariant set and stay thereafter.*

Remark 3.2 *In practical terms, the choice of μ_1^*, μ_2^* and μ_3^*, which are the upper limits of the observer parameter μ, is typically made as a result of a trade off between achieving satisfactory results, or small enough λ_1 and λ_2, and avoiding making the output feedback system too sensitive to measurement noise and avoiding possible computational difficulties. Accordingly, the user typically starts with a choice of $0 < \mu < 1$ that is not too small to start with and then keeps decreasing until a satisfactory performance is achieved.*

Remark 3.3 *The second bullet shows that the tracking error trajectories under output feedback can be made arbitrarily close to the trajectories of the target system* (25) *by choosing μ small enough. The third bullet shows that the error trajectories are ultimately bounded, and the ultimate bound $||e(t)||$ can be made arbitrarily small by choosing μ small enough.*

4 Simulation Example: Tracking Control of An Iron Pendulum in a Magnetic Field

Consider a forced oscillation of a pendulum on an elastic-plastic element shown in Figure 2. This system can be described as [37]

$$\dot{x}_1 = x_2, \tag{36}$$

$$\dot{x}_2 = -x_1 - \psi(\eta) + \sin(\omega t) + u, \tag{37}$$

$$\psi(\eta) = \sum_{i=1}^{n} p_i \eta_i, \tag{38}$$

$$\epsilon \dot{\eta}_i = \Phi_{r_i}[x_1 - \eta_i], \tag{39}$$

$$y = x_1, \tag{40}$$

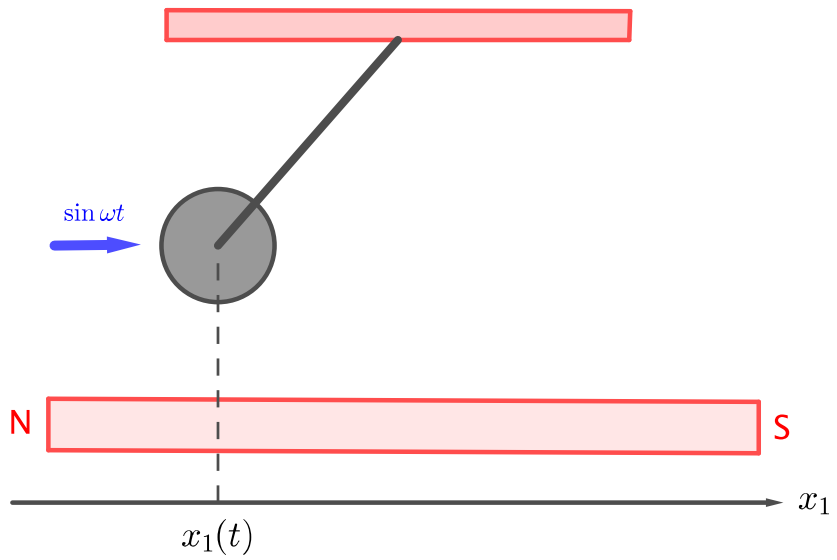

Figure 2: An iron pendulum operating within a magnetic field with an exogenous force $\sin(\omega t)$.

where $\sin(\omega t)$ is exogenous signal with frequency ω. The function $\psi(\eta)$ represents hysteresis as described in Section 2.2, from which we also recall that $p_i, i = 1, 2, \ldots, n$, $n > 0$ and $\epsilon > 0$ are modeling parameters. We consider the problem of controlling the output y so that it asymptotically tracks a reference signal d_1, where it is assumed that d_1, $d_2 \triangleq \frac{dd_1}{dt}$ and $d_3 \triangleq \frac{dd_2}{dt}$ to be bounded for all $t \geq 0$. The closed-loop system's transient response is desired to have some predefined characteristics such as particular settling time and percentage overshoot. Towards accomplishing this objective, we consider the change of variables $e = x - d$, where $e = [e_1\ e_2]^T$, $x = [x_1\ x_2]^T$, and $d = [d_1\ d_2]^T$. Using this change of variables, we get the tracking error dynamics

$$\dot{e}_1 = e_2, \tag{41}$$

$$\dot{e}_2 = -e_1 - d_1 - \psi(\eta) + \sin(\omega t) - d_3 + u, \tag{42}$$

$$\epsilon\dot{\eta}_i = \Phi_{r_i}[e_1 + d_1 - \eta_i], \tag{43}$$

$$y_t = e_1 = x_1 - d_1, \tag{44}$$

where $\psi(\eta)$ is given in (38) and y_t is the measured tracking error. Considering the system (41)-(44), the control problem can now be cast as how to design an output feedback controller to asymptotically regulate e to zero while meeting certain requirements on the transient response.

Define $\kappa \triangleq \sin(\omega t) - \psi(\eta) - d_1 - d_3$. Accordingly, the state-feedback control

$$u = -\kappa - k_1 e_1 - k_2 e_2. \tag{45}$$

This, in turn, leads to the closed-loop system

$$\dot{e} = A_c e, \tag{46}$$

$$\epsilon \dot{\eta}_i = \Phi_{r_i}[e_1 - d_1 - \eta_i], \quad i = 1, 2, \ldots, n, \tag{47}$$

where $A_c = \begin{bmatrix} 0 & 1 \\ -1 - k_1 & -k_2 \end{bmatrix}$, and k_1, k_2 are positive constants chosen so that A_c have desired eigenvalues. Notice that the matrix A_c in (46) is slightly different than that given in (25) because the function $a(x) = -x_1$ defined in (1) is known in this case.

Following the procedure outlined in Section 2, an output-feedback controller can be taken as

$$u = M \text{sat}\left(\frac{-\hat{\kappa} - k_1 e_1 - k_2 \hat{e}_2}{M}\right), \tag{48}$$

where M sets the saturation bounds as defined in the previous section. This controller is to be combined with the observer

$$\dot{\hat{e}}_1 = \hat{e}_2 + \frac{\alpha_1}{\mu}(y_t - \hat{e}_1), \tag{49}$$

$$\dot{\hat{e}}_2 = -\hat{e}_1 + \hat{\kappa} + u + \frac{\alpha_2}{\mu^2}(y_t - \hat{e}_1), \tag{50}$$

$$\dot{\hat{\kappa}} = \frac{\alpha_3}{\mu^3}(y_t - \hat{e}_1), \tag{51}$$

where $\mu > 0$ is a small parameter to be designed, and α_1, α_2 and α_3 are chosen such that the polynomial $s^3 + \alpha_1 s^2 + \alpha_2 s + \alpha_3 = 0$ is Hurwitz.

We next provide simulation results to verify the effectiveness of the control system proposed in the previous section. The system, controller and observer parameters are given by: $\omega = 2$ rad/sec, $\epsilon = 0.1, n = 2, p_1 = 0.8, p_2 = 0.4, \alpha_1 = 6, \alpha_2 = 11, \alpha_3 = 6$.

It is desired to achieve a damped transient response with a settling time less than 5 sec. This is achieved if the closed-loop system (46) has eigenvalues -1 and -2. This, in turn, can be achieved through a state-feedback control by selecting $k_1 = 1$ and $k_2 = 3$. The initial conditions are chosen as: $x_1(0) = 0.5$, $x_2(0) = 1$, $\eta_1(0) = \eta_2(0) = 0.25$, $\hat{e}_1(0) = 2$, $\hat{e}_2(0) = 1$, $\hat{\kappa}(0) = 0.75$. To determine the appropriate saturation limits, we examined the maximum values for the control signal under-

state feedback, which was found to be within ± 5. So to not let the saturation affect the dynamics of the system and guard only against peaking, we choose the saturation limits as $M = \pm 50$.

Figure 3 shows the output response of the closed-loop system in the case of state-feedback control as well as the output-feedback control for different values of μ. It is clear from Figure 3 that the output-feedback control achieves the performance obtained under state-feedback control as μ gets smaller or as the observer gets faster. Notice that when $\mu = 0.00001$ the performances under state- and output- feedback are almost indistinguishable. This shows that we can design the state-feedback controller to achieve the desired transient performance and then we can recover this performance using the observer-based controller by setting μ small enough. Figure 2 shows the output response and the control effort when the desired reference signal is time changing.

Next, we examine the case when the the reference signal has a frequency of 10 rad/sec and the hysteresis parameter is $\epsilon = 0.00001$. This case represents a faster reference signal and a faster hysteresis rate. To show that the control system can handle unknown system parameters, we assume that the coefficient of x_1 in (37), and hence e_1 in (42), is unknown. This leads to the new definition of κ as $\kappa \triangleq \sin(\omega t) - \psi(\eta) - e_1 - d_1 - d_3$. Accordingly, the observer equation (50) needs to be changed to

$$\dot{\hat{e}}_2 = \hat{\kappa} + u + \frac{\alpha_2}{\mu^2}(y_t - \hat{e}_1), \tag{52}$$

and to be used with (49), (51), and (48). To optimally choose the controller parameters, we consider the Liner Quadratic Regulator (LQR) control law that minimizes $J = \int (e^T Q e + R u^2) dt$. Using

$$A = \begin{bmatrix} 0 & 1 \\ 0 & 0 \end{bmatrix}, B = \begin{bmatrix} 0 \\ 1 \end{bmatrix}, Q = \begin{bmatrix} 1 & 0 \\ 0 & 1 \end{bmatrix}, R = 1$$

and the Matlab command `lqr` (A, B, Q, R), we get $k_1 = 1$ and $k_2 = 1.7321$. This results in the closed-loop eigenvalues $-0.866 \pm i0.5$. Notice that because we are assuming that e_1 is unknown in (42), the closed-loop matrix in (46) is given by

$$A_c = \begin{bmatrix} 0 & 1 \\ -k_1 & -k_2 \end{bmatrix}.$$

After examining the state-feedback control performance, the saturation limits were chosen to be ± 150. The simulation results of this case are shown in Figures 5 and 6. Figure 5 shows the effectiveness of the output feedback controller and the control effort while Figure 6 shows the effectiveness of the high-gain observer.

The control action, expressed in equation (32) or (48), is essentially in the form of proportional

and derivative (PD) control. This feedback-linearization PD control strategy is implemented with a high-gain observer leading to an output feedback control. This implies that by appropriately choosing the controller parameters we can add damping to the system and enhance its response speed. This observation is realizable by making the observer parameter μ sufficiently small as shown in Figure 3.

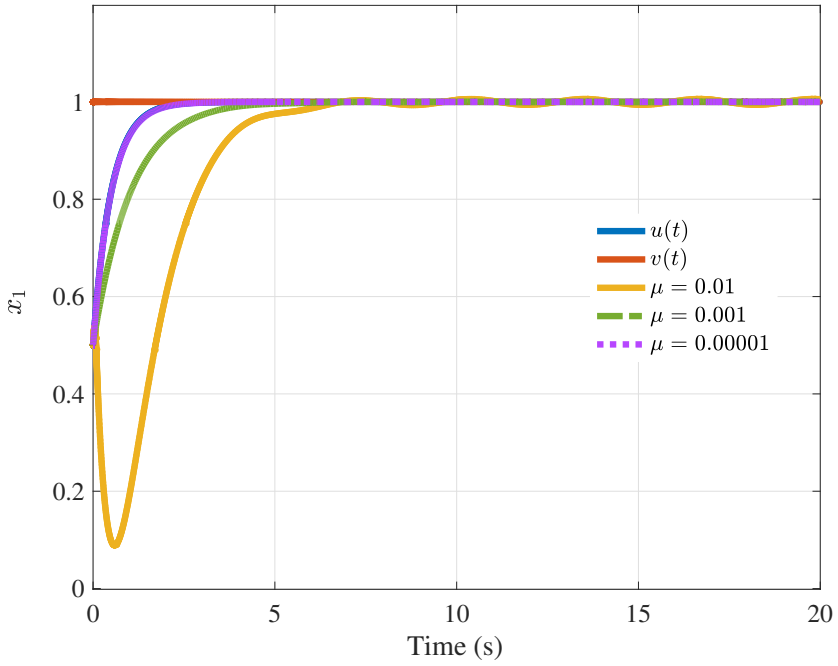

Figure 3: Output response both under state-feedback and output-feedback for different values of μ.

5 Application to a Piezoelectric Actuator

The extended high-gain observer-based feedback is proposed in this section to control a piezoelectric actuator. This section includes experimental setup, system modeling, control design, and experimental results. This actuator shows rate-dependent hysteresis, creep effects, and oscillations.

5.1 The actuator and the experimental setup

The piezoelectric actuator, displayed in Figure (7-a) and called piezotube, has a cylinder shape with internal hole. It has four external electrodes and one internal electrode for electrical ground.

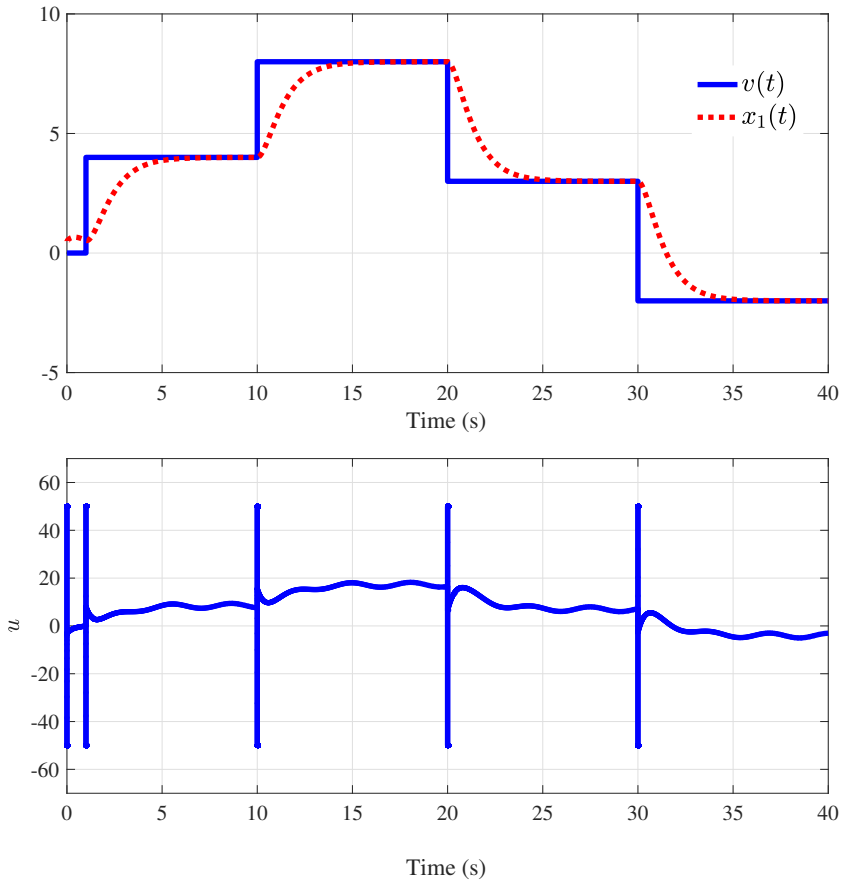

Figure 4: Output response and the control effort when the hysteresis parameter $\epsilon = 0.1$.

According to which of the four external electrodes are subjected to electrical potential (voltage), the piezotube bends along the x-axis or along the y-axis. On the other hand, if all the four external electrodes receive the same electrical potential, the actuator expands along its axis (z-axis). A piezotube actuator can therefore perform x-y-z movement. Piezotubes are classically used in precise positioning applications such as atomic force microscopes for images scanning [47] and positioners for micro- and nano-manipulation [48]. In fact piezotubes can provide high resolution (down to nanometers) and large bandwidth (up to hundreds of Hertz).

In this section we test the proposed high-gain observer-based output feedback control in the direction of y-axis. The experimental setup is displayed in Figure (7-b) and is composed of:

- **the Piezotube micropositioning actuator**: the actuator itself, referenced as PT 230.94 which has 30mm of length and 3.2 mm of external diameter. The internal hole of the piezotube has 2.2 mm of diameter. The piezotube can be driven with a voltage u up to

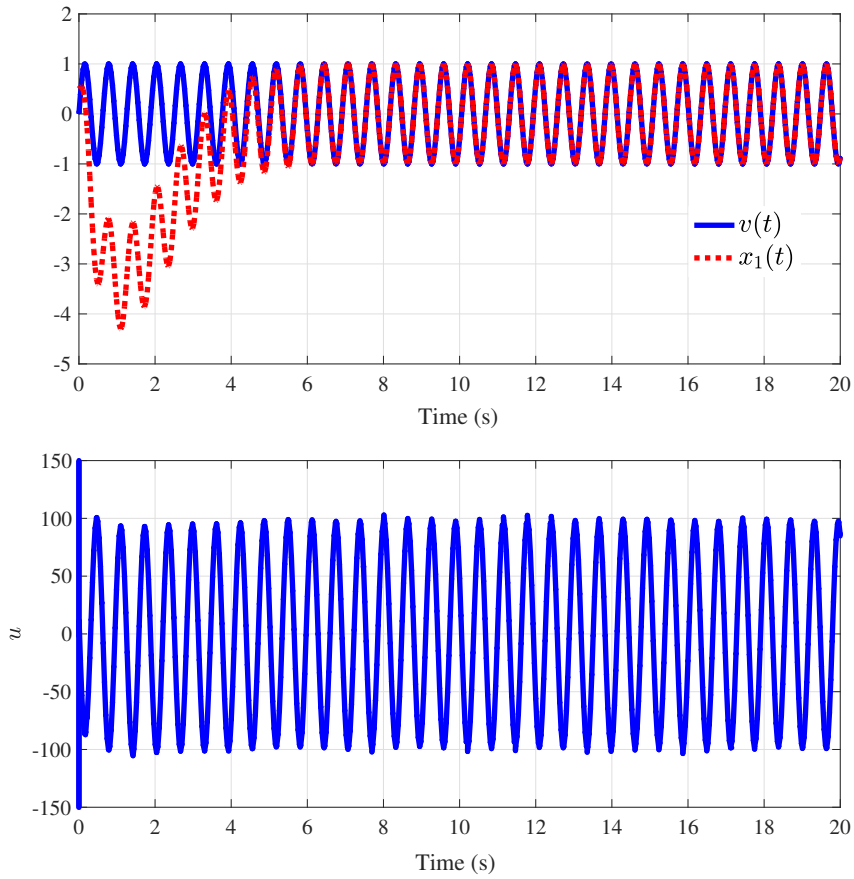

Figure 5: Output response and the control effort when the frequency of the reference signal is 10 rad/s and the hysteresis parameter $\epsilon = 0.00001$ and the observer parameter $\mu = 0.00001$.

± 200 V but we limit in this paper the operating range to ± 150 V because of the limitation of the voltage amplifier. Meanwhile, the input range of ± 150V is sufficient to observe the hysteresis of the actuator and to analysis the controller performances proposed in this paper.

- **Sensor**: an inductive sensor with its probe is placed in front of the tip of the piezotube to measure its y displacement. The sensor is the ECL202 and can provide 30 nm of resolution with a bandwidth of 15 kHz.

- **Data acquisition**: a computer with Matlab-Simulink in which the driving voltage u is generated, the measurement y is acquired and the controllers are implemented. A dSPACE acquisition board (dS1103) serves as converters between the numerical signals in the computer and the analogical signals from and to the piezotube actuator.

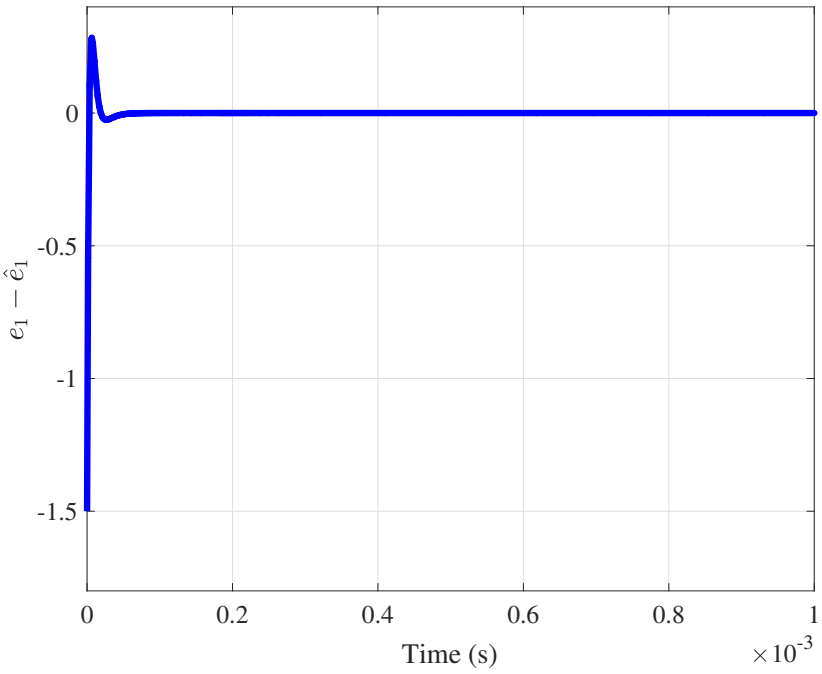

Figure 6: The estimation error $e_1 - \hat{e}_1$ when the frequency of the reference signal is 10 rad/s and the hysteresis parameter $\epsilon = 0.00001$ and the observer parameter $\mu = 0.00001$.

- **amplifier**: a high-voltage (HV) amplifier that amplifies by 20 times the voltage from the computer-dSPACE board, limited to ± 10 V.

5.2 Actuator dynamics

In order to obtain the piezotube actuator dynamics, first we apply a sinusoidal input (driving) voltage. An amplitude of 150 V has been used at different excitation frequencies between 0.1 Hz and 200 Hz. Figure 8 shows the obtained displacement versus the input voltage over different excitation frequencies. Beyond the hysteresis nonlinearity property and the fact that its shape changes versus the frequency (rate-dependency), it shows that the range of displacement is about ± 30 μm for a voltage of ± 150 V, i.e. the gain is $5[\frac{\mu m}{V}]$. Such a gain is high and thus interesting when comparing to other piezoelectric cantilevered actuators devoted to precise positioning tasks [2]. Then, we apply a step input voltage of 150 V to the piezotube. The measured output displacement is depicted in Figure 9, which clearly shows the badly damped oscillations property. A quick identification shows that the first resonant frequency is of 776Hz and the settling time

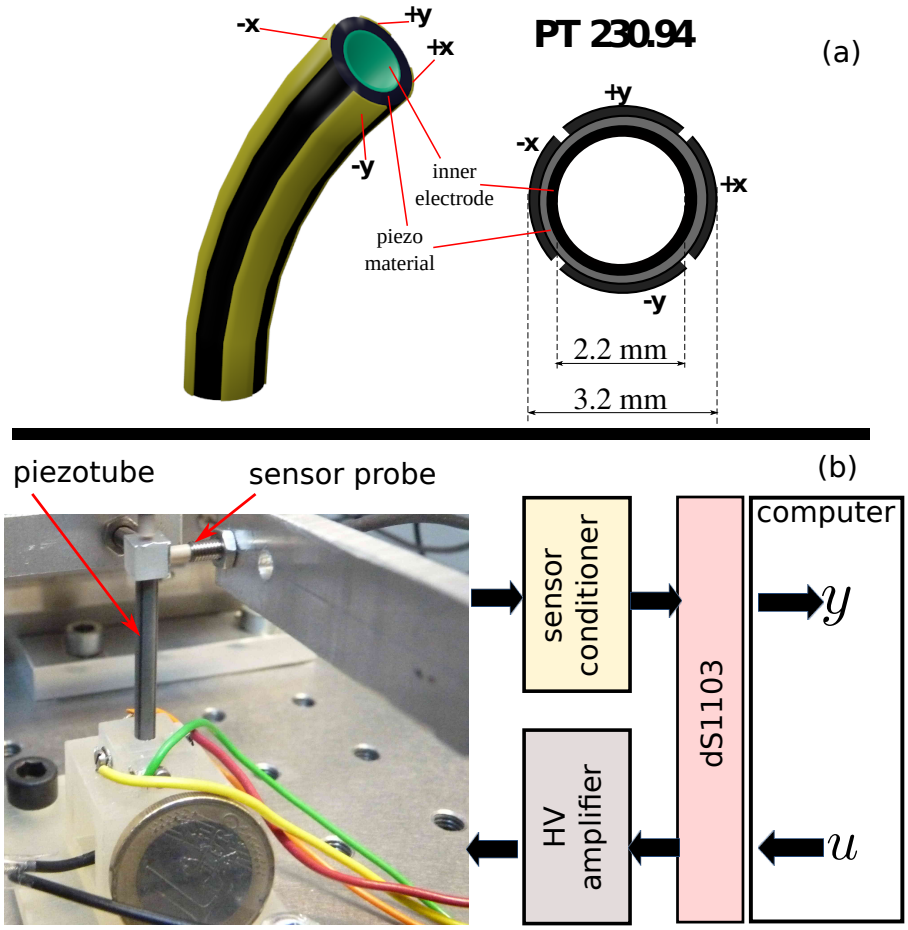

Figure 7: (a) the piezotube actuator used in the experiment, and (b) the experimental setup.

is approximately 19 ms. Moreover, the response shows a low-rate drift (can be seen at 0.1 Hz in Figure 8). This drift is called creep phenomenon and is typical for piezoelectric actuators. Similar to hysteresis, the creep phenomenon introduces precision loss in the tasks to be carried out and should therefore be controlled.

In this section we consider the following system to model the nonlinear dynamics of the piezotube actuator

$$\dot{x}_1 = x_2 \tag{53}$$

$$\dot{x}_2 = -a_2 x_2 - a_1 x_1 + \mathcal{P}(u, \eta) + \xi, \tag{54}$$

where $\xi(t)$ represents bounded unknown disturbances and unmodelled dynamics, $\mathcal{P}(u, \eta) = p_0 u + \sum_{i=1}^{n} p_i \eta_i$, $\epsilon \dot{\eta}_i = \Phi_{r_i}[u - \eta_i]$, and $y(t) = x_1(t)$. It is important to mention that we consider uncertain hysteresis and creep nonlinearities with second order system to present the oscillations of the

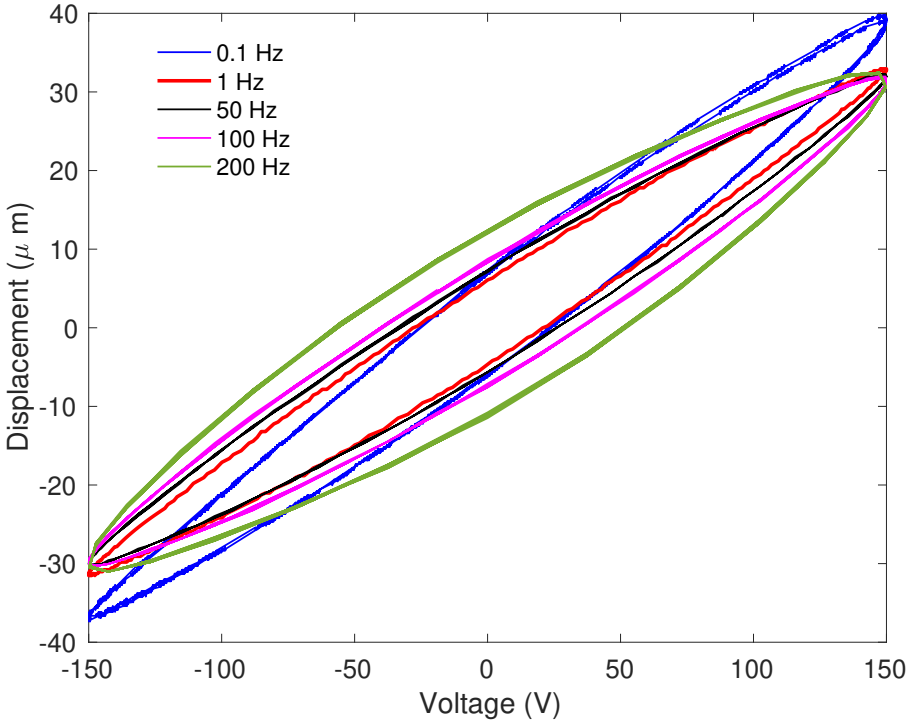

Figure 8: Measured hysteresis loops of the piezoelectric cantilever actuator under a sinusoidal voltage with $150V$ of amplitude at 0.1 Hz, 1 Hz, 50 Hz, 100 Hz, and 200 Hz.

piezotube actuator. Notice that the hysteresis model in this case depends on u. The parameters of the model are $a_1 = 23903519, a_2 = 293$, and $p_0 = 2511930$. More details about the system (53)-(54) can be found in [21] and [49].

5.3 Output-feedback Controller

Following the procedure outlined in Section 3.2, an extended high-gain observer can be designed in the form of

$$\dot{\hat{e}}_1 = \hat{e}_2 + \frac{\alpha_1}{\mu}(y_t - \hat{e}_1) \tag{55}$$

$$\dot{\hat{e}}_2 = -a_1\hat{e}_1 - a_2\hat{e}_2 + \hat{\kappa} + p_0 u + \frac{\alpha_2}{\mu^2}(y_t - \hat{e}_1) \tag{56}$$

$$\dot{\hat{\kappa}} = \frac{\alpha_3}{\mu^3}(y_t - \hat{e}_1), \tag{57}$$

where $y_t = e_1 = y - d_1$ and d_1 is the desired input. The observer parameters are chosen to be $\alpha_1 = 6, \alpha_2 = 11, \alpha_3 = 6$, and $\mu = 0.00001$. It is important to note here that $\hat{\kappa}$ now provides an

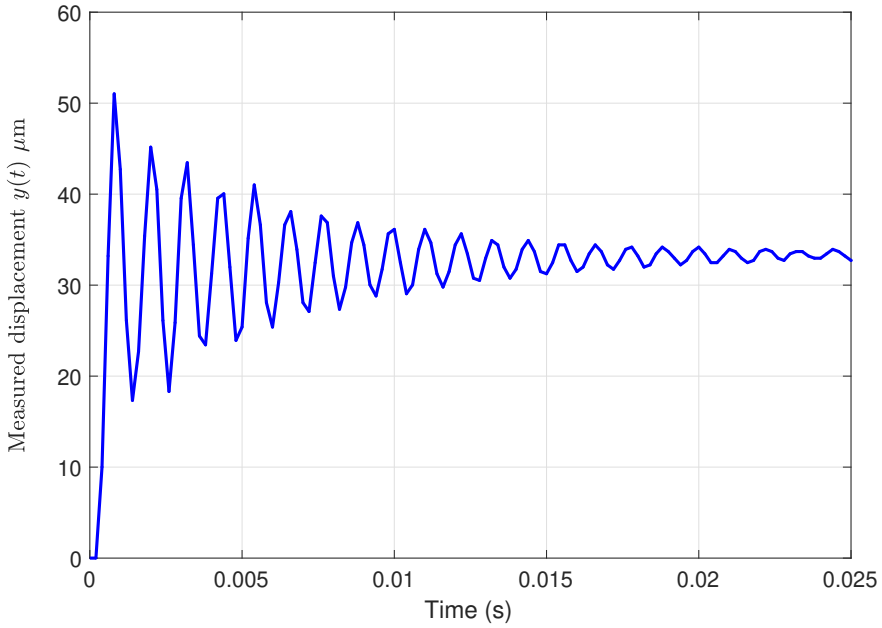

Figure 9: Step response of the actuator with $150V$ of input voltage.

estimate of $\sum_{i=1}^{n} p_i\eta_i - a_1d_1 - a_2d_2 - d_3$, where d_2 and d_3 are the first and second derivatives of d_1, respectively. The estimates from (55)-(57) will then be used in

$$u = \frac{M}{p_0}\text{sat}\left(\frac{-\hat{\kappa} - k_1e_1 - k_2\hat{e}_2}{M}\right). \tag{58}$$

The saturation level is chosen to be $M = \pm 500$ to be sure that it will not saturate the experimental driving voltage and thus create unwanted oscillations. The controller gains are chosen as $k_1 = 900000000, k_2 = 0$. These gains were chosen as initial setting, however they can be tuned afterwards for better performances of the closed-loop if required. The output-feedback controller is afterwards applied to the experimental piezotube actuator.

First a series of step input as reference y_{ref} is applied to the closed-loop which includes the piezotube actuator. Figure 10 presents the results where the output y is compared with the desired displacement y_{ref}. As we can observe, the output tracks the input reference and no creep (drift) appears in the output displacement and the oscillations are damped. Then, a varying input desired displacement is applied to verify tracking performance with a different desired input displacement. Figure 11-a displays the results when the desired displacement varies between $-30\mu m$ to $30\mu m$. Figure 11-b shows the tracking error and the which the root-mean-square of the tracking error is $0.326\mu m$.

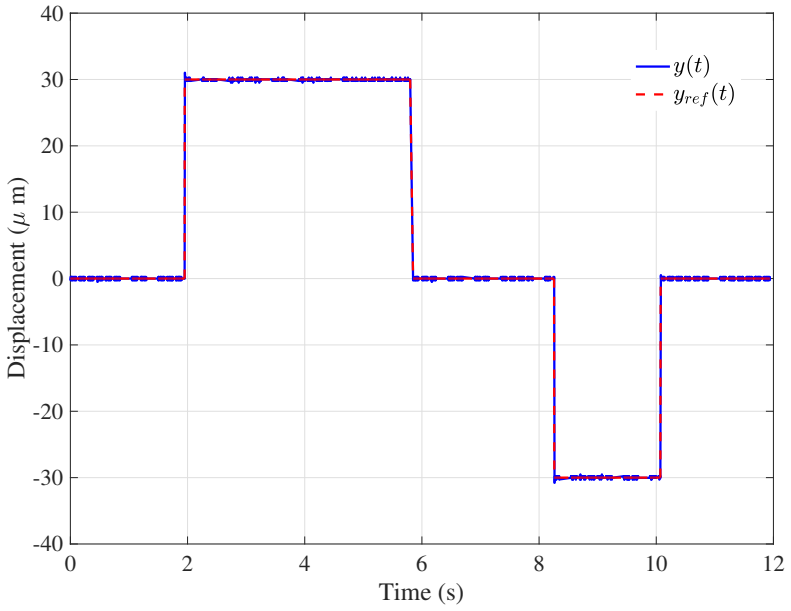

(a)

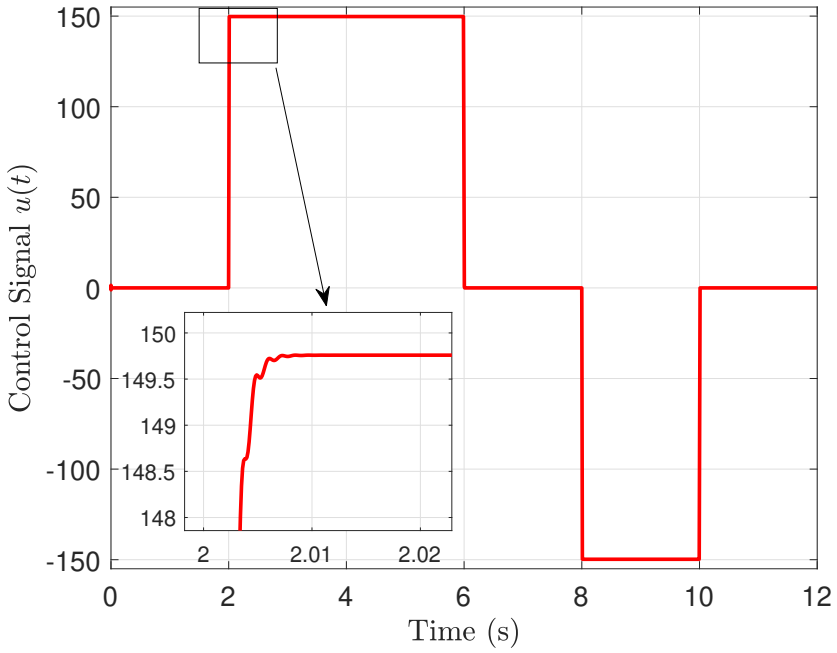

(b)

Figure 10: (a) Comparison between the desired step displacement and output displacement with proposed control signal (58), (b) the control signal of the proposed technique in (58).

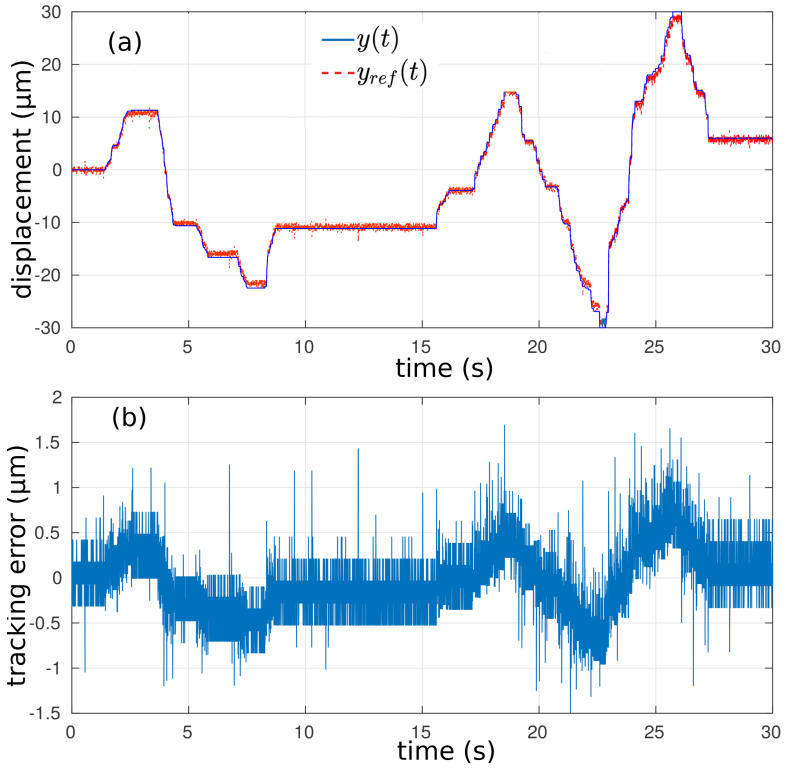

Figure 11: Tracking performance of the proposed control system (54) with a varying signal: (a) comparison between the desired and output displacement with the proposed control (58), (b) tracking error of (a).

The time domain performances of the closed-loop with the proposed controller (58) is analyzed through a step response (desired displacement). Figure 12 shows the measured step response and the simulated step response when a desired displacement of $30\mu m$ is applied. In order to compare the performances of the proposed controller (58) with those in the literature, we considered the feedforward-feedback controller of the same piezotube actuator that is recently proposed in [50]. In [50], the hysteresis is compensated with the inverse rate-dependent Prandtl-Ishlinskii hysteresis compensator and a Reference Signal Tracking structured designed with interval techniques. As depicted in Figure 12, the proposed closed-loop technique has better response time than the closed-loop control in [50]. The proposed controller exploits the internal dynamics of the actuator (state estimation) and this allows to perform better dynamics in the closed-loop systems.

Then a harmonic analysis is performed. A sinusoidal shaped desired displacement y_{ref} with an amplitude of $30\mu m$ and an excitation frequency between $\approx 1.5Hz$ $(10\frac{rad}{s})$ and $1.7KHz$ $(10681\frac{rad}{s})$ is used. Figure 13 illustrates the resulting magnitude, the magnitude of the open-loop, and the magnitude of the closed-loop with the feedforward-feedback controller in [50]. The results

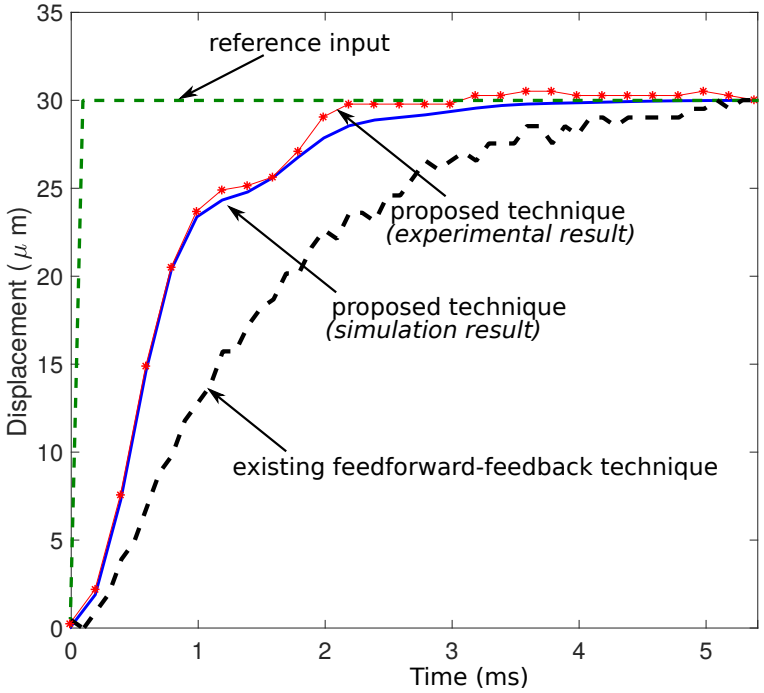

(a)

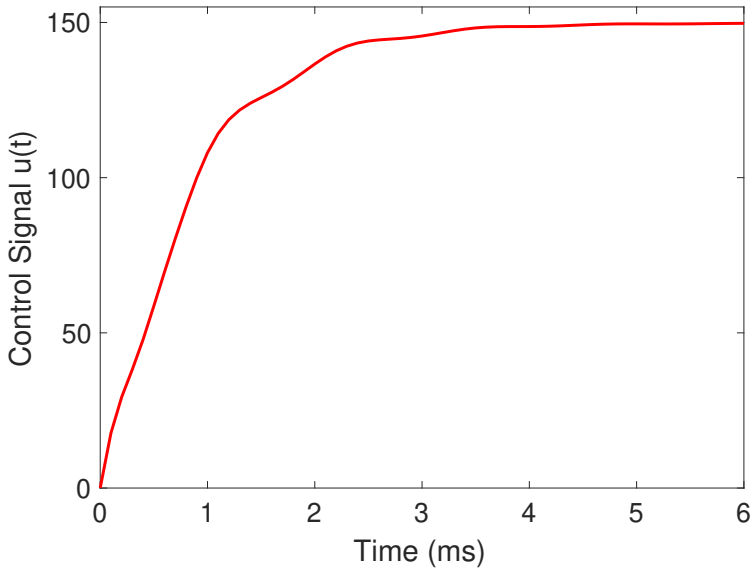

(b)

Figure 12: (a) Comparison between step desired displacement and output displacement with the proposed inversion-free control signal (58) and inversion-based control technique in [50], (b) the control signal of the proposed technique in (58).

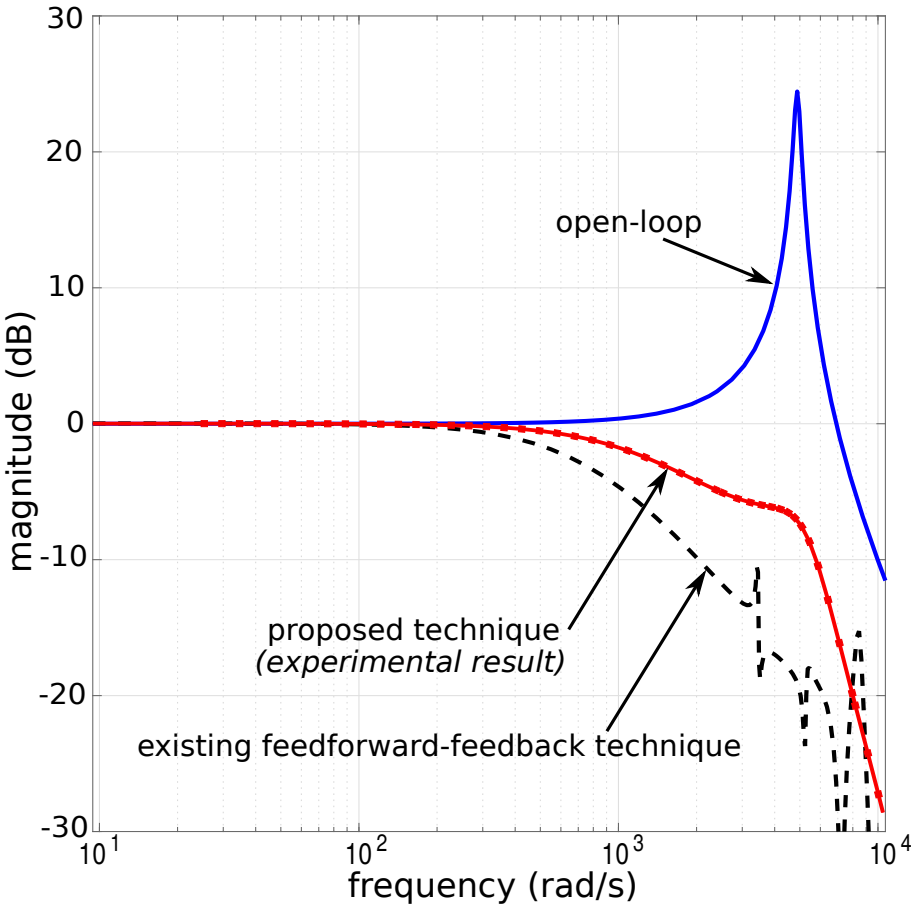

Figure 13: The frequency responses of the piezotube actuator with and without control system and with inversion-based control technique in [50].

show that the resonance at $776Hz$ ($4880\frac{rad}{s}$) is damped by the two closed-loop control systems (the proposed extended high-gain observer-based control and the feedforward-feedback controller). However, the proposed extended high-gain observer-based control approach shows a higher bandwidth.

As mentioned in Section 4, the control action is designed based on feedback linearization and takes the form of proportional-derivative (PD) control. The role of the high-gain observer is to implement this strategy based only on feedback of the output. So by appropriately choosing the controller parameters we can add damping to the system and enhance its response speed. This is exactly what we observe in Figure 12. Moreover, the controller in this case can add more bandwidth to the system as shown in Figure 13. This is possible thanks to the high-gain nature of the observer which can recover the performance of the state-feedback controller by making the observer gain sufficiently high.

6 Conclusions

We show that, for motion systems with uncertain hysteresis as in the case of an iron pendulum in a magnetic field and piezoceramic micro-positioing actuator, it is possible to follow an extended high-gain observer-based approach to solve the output feedback tracking problem. In this way, one can first design a feedback linearzing control, assuming that all the states and the model information are available, to shape the transient response of the closed-loop system. An extended high-gain observer can then be utilized to provide the missing information in a relatively fast time. As a result, it is possible for the output feedback controller to robustly recover the performance of the state feedback controller. It is important to mention that the proposed feedback controller of this study assumes uncertain hysteresis nonlinearities and partially known linear dynamics.

Acknowledgement

This work was supported by the Natural Sciences and Engineering Research Council of Canada and French Embassy in Canada.

References

[1] R. Smith, "Smart material systems: model development," Society for Industrial and Applied Mathematics, 2005.

[2] M. Rakotondrabe, *Smart materials-based actuators at the micro/nano-scale: characterization, control and applications*. Springer, New York, 2013.

[3] K. Leang and A. Fleming, *Design, modeling and control of nanopositioning systems*. Springer, 2018.

[4] J. Crews, N. Bravo, and R. Smith, "Model Development for PZT Bimorph Actuation Employed for Micro-air Vehicles," in *ASME 2016 Conference on Smart Materials, Adaptive Structures and Intelligent Systems*, pp. 1–6, 2016.

[5] S. Wen and Q. Xu, "Design of a novel piezoelectric energy harvester based on integrated multi-stage force amplification frame," *IEEE/ASME Transactions on Mechatronics*, vol. 24, 2019.

[6] F. Stefanski, B. Minorowicz, J. Persson, A. Plummer, and C. Bowen, "Non-linear Control of a Hydraulic Piezo-valve Using a Generalised Prandtl–Ishlinskii hysteresis Model," *Mechanical Systems and Signal Processing*, vol. 82, pp. 412–431, 2017.

[7] F. J. Salvador, A. H. Plazas, J. Gimeno, and M. Carreres, "Complete Modelling of a Piezo Actuator Last-generation Injector for Diesel Injection Systems," *International Journal of Engine Research*, vol. 15, no. 1, pp. 3–19, 2014.

[8] S. Lescano, M. Rakotondrabe, and N. Andreff, "Precision Prediction Using Interval Exponential Mapping of a Parallel Kinematic Smart Composite Microstructure," in *International Conference on Intelligent Robots and Systems*, pp. 1994–1999, 2015.

[9] P. Liu, P. Yan, and H. Özbay, "Design and Trajectory Tracking Control of a Piezoelectric Nano-manipulator with Actuator Saturations," *Mechanical Systems and Signal Processing*, vol. 111, pp. 529–544, 2018.

[10] Z.-c. Qiu, B. Wang, X.-m. Zhang, and J.-d. Han, "Direct Adaptive Fuzzy Control of a Translating Piezoelectric Flexible Manipulator Driven by a Pneumatic Rodless cylinder," *Mechanical Systems and Signal Processing*, vol. 36, no. 2, pp. 290–316, 2013.

[11] Y.-J. Li, J. Zhang, Z.-Y. Jia, and M. Qian, "A Novel Piezoelectric 6-Component Heavy Force/moment 6ensor for Huge Heavy-load Manipulator's Gripper," *Mechanical Systems and Signal Processing*, vol. 23, no. 5, pp. 1644–1651, 2009.

[12] S. Devasia, E. Eleftheriou, and R. Moheimani, "A survey of control issues in nanopositioning," *IEEE Transactions on Control Systems Technology*, vol. 15, pp. 802–823, 2007.

[13] M. Rakotondrabe, "Bouc-wen modeling and inverse multiplicative structure to compensate hysteresis nonlinearity in piezoelectric actuators," *IEEE Transactions on Automation Science and Engineering*, vol. 8, pp. 428–431, 2011.

[14] M. Al Janaideh, S. Rakheja, and C. Su, "An analytical generalized prandtl–ishlinskii model inversion for hysteresis compensation in micropositioning control," *IEEE/ASME Transactions on mechatronics*, vol. 16, pp. 734–744, 2010.

[15] X. Tan and J. S. Baras, "Modeling and control of hysteresis in magnetostrictive actuators," *Automatica*, vol. 40, pp. 1469–1480, 2004.

[16] X. Tan and J. S. Baras, "Adaptive identification and control of hysteresis in smart materials," *IEEE Transactions on Automatic Control*, vol. 50, pp. 827–839, 2005.

[17] M. A. Janaideh, C.-Y. Su, and S. Rakheja, "Inverse compensation error of the prandtl-ishlinskii model," *51st IEEE Conference on Decision and Control*, pp. 1597–1602, 2012.

[18] L. Riccardi, D. Naso, B. Turchiano, and H. Janocha, "Design of linear feedback controllers for dynamic systems with hysteresis," *IEEE Transactions on Control Systems Technology*, vol. 22, pp. 1268–1280, 2013.

[19] M. Al Janaideh and P. Krejci, "Inverse rate-dependent prandtl–ishlinskii model for feedforward compensation of hysteresis in a piezomicropositioning actuator," *IEEE/ASME Transactions on Mechatronics*, vol. 18, pp. 1498–1507, 2013.

[20] M. Al Janaideh and O. Aljanaideh, "Further results on open-loop compensation of rate-dependent hysteresis in a magnetostrictive actuator with the prandtl-ishlinskii model," *Mechanical Systems and Signal Processing*, vol. 104, pp. 835–850, 2018.

[21] M. Al Janaideh, M. Rakotondrabe, and O. Aljanaideh, "Further results on hysteresis compensation of smart micropositioning systems with the inverse prandtl-ishlinskii compensator," *IEEE Transactions on Control Systems Technology*, vol. 24, pp. 428–439, 2016.

[22] L. Riccardi, D. Naso, B. Turchiano, and H. Janocha, "Design of linear feedback controllers for dynamic systems with hysteresis," *IEEE Transactions on Control Systems Technology*, vol. 22, pp. 1268–1280, 2014.

[23] A. El-Shaer, M. Al Janaideh, P. Krejci, and M. Tomizuka, "Robust performance enhancement using disturbance observers for hysteresis compensation based on generalized prandtl–ishlinskii model," *Journal of Dynamic Systems, Measurement, and Control*, vol. 135, pp. 1–13, 2013.

[24] D. Chowdhury, Y. K. Al-Nadawi, and X. Tan, "Hysteresis compensation using extended high-gain observer and dynamic inversion," in *ASME Dynamic Systems and Control Conference*, pp. 6821–6826, 2018.

[25] M. Al Janaideh and A. El-Shaer, "Performance enhancement for a class of hysteresis nonlinearities using disturbance observers," *International Journal of Control, Automation and Systems*, vol. 12, pp. 283–293, 2014.

[26] M. Al Janaideh, R. Naldi, L. Marconi, and P. Krejci, "A hybrid system for a class of hysteresis nonlinearity: modeling and compensation," in *Proceedings of the IEEE Conference on Decision and Control*, pp. 5380–5385, Maui, HI, 2012.

[27] M. A. Janaideh and D. S. Bernstein, "Adaptive Control of Uncertain Hammerstein Systems with Hysteretic Nonlinearities," in *53rd IEEE Conference on Decision and Control*, pp. 545–550, 2014.

[28] R. Gorbet, K. Morris, and D. Wang, "Passivity-based stability and control of hysteresis in smart actuators," *IEEE Transactions on control systems technology*, vol. 9, pp. 5–16, 2001.

[29] M. Al Janaideh, M. Rakotondrabe, I. Darabsah, and O. Aljanaideh, "Internal model-based feedback control design for inversion-free feedforward rate-dependent hysteresis compensation of piezoelectric cantilever actuator," *Control Engineering Practice*, vol. 72, pp. 29–41, 2016.

[30] M. Al Janaideh and D. S. Bernstein, "Adaptive control of uncertain hammerstein systems with hysteretic nonlinearities," in *IEEE Conference on Decision and Control*, pp. 545–550, 2014.

[31] Y. BAl Hamidi and M. Rakotondrabe, "Feedforward and output feedback control of a highly oscillating and nonlinear 2-dof piezoelectric actuator by using input shaping compensator and a linear quadratic regulator," *SPIE Sensing Technology+Applications; Sensors for Next Generation Robots*, vol. doi:10.1117/12.2229008, 2016.

[32] M. Hammouche, P. Lutz, and M. Rakotondrabe, "Robust and optimal output-feedback control for interval state-space model: Application to a two-degrees-of-freedom piezoelectric tube actuator," *ASME ournal of Dynamic Systems, Measurement and Control*, vol. 141, no. 2, p. 021008, 2018.

[33] M. Hammouche, P. Lutz, and M. Rakotondrabe, "Robust and guaranteed output-feedback force control of piezoelectric actuator under temperature variation and input constraints," *Asian Journal of Control*, vol. doi.DOI:10.1002/asjc.2258, 2019.

[34] F. Giri, J. Gning, and F. Chaoui, "Adaptive output feedback control of bouc-wen hysteretic systems," *IFAC Proceedings*, vol. 43, pp. 1–6, 2010.

[35] M. Al Janaideh and A. Boker, "Modeling and output-feedback control of systems with netushil rate-dependent hysteresis nonlinearties," in *IEEE Conference on Decision and Control*, pp. 6912–6917, 2018.

[36] H. K. Khalil, *Noninear systems*. Prentice-Hall, New Jersey, 1996.

[37] M. Mortell, R. O'Malley, A. Pokrovskii, and V. Sobolev, *Singular perturbations and hysteresis*. Society for Industrial and Applied Mathematics, 2005.

[38] C. Kuehn and C. Munch, "Generalized play hysteresis operators in limits of fast-slow systems," *SIAM Journal on Applied Dynamical Systems*, vol. 16, pp. 1650–1685, 2017.

[39] P. Krejci, M. A. Janaideh, and F. Deasyi, "Inversion of hysteresis and creep operators," *Smart Materials and Structures*, vol. 407, pp. 1354–1356, 2012.

[40] M. A. Janaideh and P. Krejci, "A rheological model for the rate-dependent prandtl-ishlinskii model," *52nd IEEE Conference on Decision and Control*, vol. 407, pp. 6646–6651, 2013.

[41] H. K. Khalil, *High-gain observers in nonlinear feedback control*. SIAM, 2017.

[42] A. M. Boker and H. K. Khalil, "Nonlinear observers comprising high-gain observers and extended kalman filters," *Automatica*, vol. 49, no. 12, pp. 3583–3590, 2013.

[43] A. M. Boker and H. K. Khalil, "Semi-global output feedback stabilization of non-minimum phase nonlinear systems," *IEEE Transactions on Automatic Control*, vol. 62, no. 8, pp. 4005–4010, 2016.

[44] A. M. Boker and H. K. Khalil, "Control of flexible joint manipulators using only motor position feedback: A separation principle approach," in *52nd IEEE Conference on Decision and Control*, pp. 244–249, IEEE, 2013.

[45] F. Esfandiari and H. Khalil, "Output feedback stabilization of fully linearizable systems," *International Journal of control*, vol. 56, pp. 1007–1037, 1992.

[46] L. Freidovich and H. Khalil, "Performance recovery of feedback-linearization-based designs," *IEEE Transactions on Automatic Control*, vol. 53, pp. 2324–2334, 2008.

[47] G. Binnig and D. Smith, "Single-tube three-dimensional scanner for scanning tunneling microscopy," *Review of Scientific Instruments*, vol. 57, pp. 1688–1689, 1986.

[48] H. Xie, M. Rakotondrabe, and S. Regnier, "Characterizing piezoscanner hysteresis and creep using optical levers and a reference nanopositioning stage," *Review of Scientific Instruments*, vol. 80, 2009.

[49] M. Al Janaideh, M. Rakotondrabe, I. Darabsah, and O. Aljanaideh, "Internal model-based feedback control design for inversion-free feedforward rate-dependent hysteresis compensation of piezoelectric cantilever actuator," *Control Engineering Practice*, vol. 72, pp. 29–41, 2016.

[50] M. Rakotondrabe and M. Al Janaideh, "An RST control design based on interval technique for piezomicropositoning systems with rate-dependent hysteresis nonlinearities," in *IEEE Conference on Decision and Control*, pp. 6821–6826, 2019.